Asian Journal of Chemistry; Vol. 36, No. 5 (2024), 1093-1100

ASIAN JOURNAL OF CHEMISTRY

https://doi.org/10.14233/ajchem.2024.31323

Synthesis, Crystal Structure, Hirshfeld Surface, Energy Frame Work and DFT Analysis of Ethyl-4-aminobenzoate Oxalate Monohydrate Salt

N.K. MANJUNATHA[1,*], K. SRINIVASA RAO[2], N. RANJEETH[1], A. SUVITHA[3], M. MANJUNATHA[4], S. SUNIL[5], S. MADAN KUMAR[6], B.P. SIDDARAJU[7], S. SHIVRAJKUMAR[8] and NABIL NAJIB ALZUBAIDY[9]

[1]Department of Chemistry, Sri Venkateshwara College of Engineering, Bangalore-562157, India
[2]Department of Mathematics, Sri Venkateshwara College of Engineering, Bangalore-562157, India
[3]Department of Physics, CMR Institute of Technology, Bengaluru-560037, India
[4]Department of Chemistry, East Point College of Engineering, Bangalore-560049, India
[5]Department of Mechanical Engineering, Sri Venkateshwara College of Engineering, Bangalore-562157, India
[6]Department of Chemistry-BMC, University of Uppsala, Husargatan 3, Uppsala, 75237, Sweden
[7]Department of Chemistry, Cauvery Institute of Technology, Mandya-571402, India
[8]Department of Chemistry, Don Bosco Institute of Technology, Bengaluru-560074, India
[9]Physics and Basic Science Department, Faculty of Engineering Technology, Albalqa Applied University, Amman 11134, Jordan

*Corresponding author: E-mail: manjunatha.nk16@gmail.com

Received: 2 February 2024; *Accepted*: 19 March 2024; *Published online*: 30 April 2024; AJC-21614

Using the single crystal X-ray diffraction method, the title molecule ethyl-4-aminobenzoate oxalate monohydrate has been synthesized, crystallized and characterized. The Hirshfeld surfaces computational approach was used to analyze the intermolecular interactions in the crystal structure. The aforementioned compound crystallizes in a monoclinic crystal system of space group $P2_1/c$ with the following cell parameters: a = 15.475(3), b = 5.7117(9), c = 14.029(3), = 101.764(6)º, V = 1214.0(4) 3 and Z = 4. The molecules in the crystal structure are connected by the N1-H1C···O7, O5-H2···O3, O7-H1···O4 and C8-H8A···Cg type intermolecular interaction, where Cg is the centroid of the ring. For the title molecule, the inter contact O···H (48.4%) contributes more to the Hirshfeld surfaces. The proton transfer from oxalic acid's phenolic group to ethyl-4-aminobenzoate's amine group, which results in the creation of salt, is revealed by the crystal structure. The ground state of ethyl-4-aminobenzoate oxalate monohydrate was also studied theoretically using the density functional method (DFT/B3LYP) with a basis set of 6–311++G(d,p). Charge transfer happens within the molecule, as shown by the computed HOMO and LUMO energies, DOS and MESP, as well as by the optimized molecular structure, electronic structural analysis and UV spectrum analysis.

Keywords: Ethyl-4-aminobenzoate, Crystal structure, Intermolecular interaction, Hirshfeld surfaces, Electrostatic potential surface.

INTRODUCTION

Benzocaine or ethyl-4-aminobenzoate ($C_{16}H_{15}N_3O_9$), is a *p*-aminobenzoic acid ester that has anaesthetic properties but lacks procaine's terminal diethyl amino group. It binds to the sodium channel and reversibly settles the neuronal layer, reducing its permeability to sodium ions. The thermal, electrical, optical and structural properties of a new symmetrical azomethine compound derived from poly(1,4-butate-diol)*bis*(4-aminobenzoate) has been reported [1]. In order to verify the existence of conformers, pinpoint their electronic transitions, vibrational linkages, structures and ionization energies, an integrated theoretical and experimental investigation of the molecule of ethyl-4-aminobenzoate is reported [2]. Computational physics is crucial to understanding crystal packing and molecular characteristics in crystal engineering. Understanding the intermolecular interactions [3-5] is aided by computational methods for Hirshfeld surfaces and quantum characteristics can be examined *via* DFT analysis [6]. The solid-state properties of pharmaceutical salts, which depend on the couterion used to generate the salt, are crucial for the development of a stable dosage form [7]. Ethyl-4-aminobenzoate oxalate monohydrate

salt was synthesized and characterized using a combination of experimental and computational techniques in order to better understand the relationship between counterion and salt characteristics.

EXPERIMENTAL

The necessary chemicals and solvents were purchased from Sigma-Aldrich, USA.

Synthesis: Oxalic acid (0.0900 g) and ethyl-4-aminobenzoate (0.1651 g) were dissolved in methanol separately and then the two solutions were combined and well agitated for 5 h. After that, the reaction mixture was allowed for a slow evaporation process, which produced crystals after few days (**Scheme-I**).

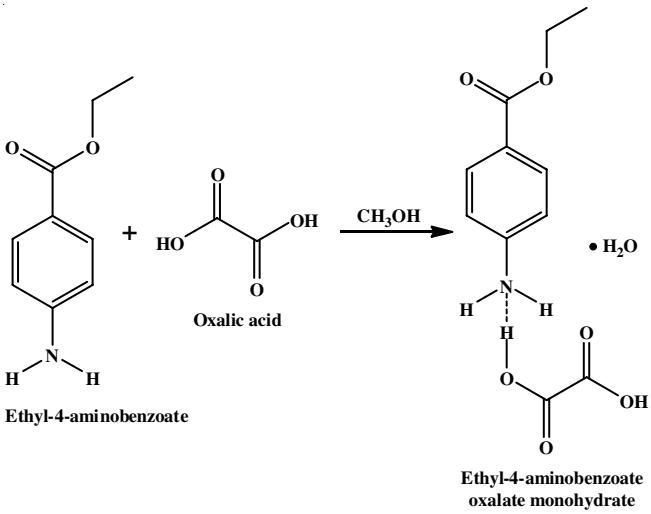

Scheme-I: Synthetic route of ethyl-4-aminobenzoate oxalate monohydrate salt

RESULTS AND DISCUSSION

Single crystal X-ray diffraction: The title compound was initially screened for crystal diffraction (diffraction and cell parameters) using Rigaku X taLab-mini diffractometer using graphite monochromated Mo-*K*α Radiation at 100 K equipped with Mo-*K*α radiation (λ = 0.71073 Å). CRYSTALCLEAR SM-EXPERT software was used to collect entire X-ray data [8]. The SHELXS and SHELXL programmes were used to solve the structure using direct methods and refined it using the full-matrix least squares method on F^2 [9]. All the non-hydrogen atoms were revealed in the first difference Fourier map itself. A riding model was used to refine the geometric positions of all the hydrogen atoms. The final difference Fourier map indicated peaks with no chemical relevance after ten cycles of refining. The geometrical calculations were carried out using the program PLATON [10]. Using the software MERCURY, molecular and packing diagrams were generated [11]. Table-1 provides information on the crystal structure and data refining. Fig. 1 depicts the ORTEP [12] of the molecule with thermal ellipsoids drawn with a 50% probability.

Hirshfeld surfaces: The Hirshfeld surfaces computational approach is used to quantify and visualize the intermolecular interactions that are present in the crystal structures [13-15].

TABLE-1
CRYSTAL DATA AND REFINEMENT STATISTICS

CCDC No.	2089478
Empirical formula	$2(C_9H_{12}NO_2)$ $2(C_2HO_4)\cdot H_2O$
Formula weight	528.46
Temperature (K)	100(2)
Crystal system	Monoclinic
Space group	P2/c
a (Å)	15.475(3)
b (Å)	5.7117(9)
c (Å)	14.029(3)
α (°)	90
β (°)	101.764(6)
γ (°)	90
Volume (Å)^3	1214.0(4)
Z	4
ρ_{calc} (g/cm^3)	1.446
μ (mm^{-1})	0.121
F(000)	556.00
Crystal size (mm^3)	0.16 × 0.12 × 0.12
Radiation	Mo*K*α (λ = 0.71073 Å)
2θ range for data collection (°)	2.69 to 30.4
Index ranges	-21 ≤ h ≤ 21, -8 ≤ k ≤ 8, -19 ≤ l ≤ 19
Reflections collected	11111
Independent reflections	2912 [R_{int} = 0.0473, R_{sigma} = 0.0423]
Data/restraints/parameters	2912/0/178
Goodness-of-fit on F2	1.010
Final R indexes [I > = 2σ(I)]	R1 = 0.0606, wR2 = 0.1607
Final R indexes [all data]	R1 = 0.1135, wR2 = 0.1975
Largest diff. peak/hole (e Å^{-3})	0.482/-0.439

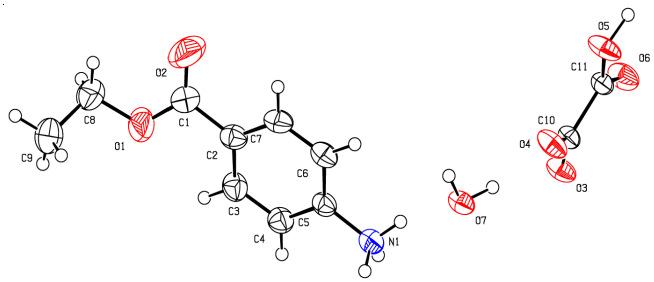

Fig. 1. The ORTEP view of ethyl-4-aminobenzoate oxalate monohydrate salt

The calculated intercontacts percentages are displayed in the figure along with 2D finger print plots. Conventional mapping of d_{norm} on molecular Hirshfeld surfaces highlights the Hirshfeld surfaces with electrostatic potential are also plotted.

3D energy frameworks: The 3D energy framework and intermolecular interaction energies were computed, visualized and analyzed using the latest version of Crystal Explorer 17 [16] software using CIF as input. By creating a cluster around the molecule with a radius of 3.8, the single point molecular wave function at the B3LYP/6-31G (d,p) level of theory is utilized to compute the energy. By using crystallographic symmetry processes, the nearby molecules in the shell around the core molecule are produced [17,18].

Crystal and molecular structure: The multi-component medicinal salt crystal structure, as shown by the X-ray diffraction investigation, crystallizes in the monoclinic crystal system with centrosymmetric *P*21/*c* space group. The asymmetric unit comprises the three different molecules namely 4-(ethoxy

carbonyl)benzenaminium, carboxyformate and water. Fig. 1 shows the ORTEP for the molecular salt drawn with a 50% probability.

All the bond distances and angles are within the normal limits. In title compound, the ethoxy moiety of carbonyl-benzenaminium is the derivative from the phenyl ring with a dihedral angle of 55.09º, whereas the carboxyfomate molecule is positioned almost axially to the phenyl ring of 4-(ethoxy-carbonyl)benzenaminium unit. The dihedral angle between the planes of the aryl ring and carboxyformate is 80.77º. This orthogonality, will help the molecular architecture to grow three dimensionally in space is shown in Fig. 2.

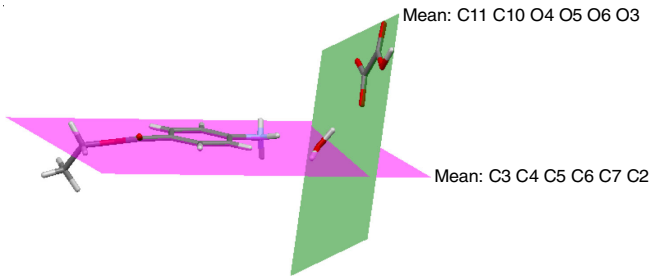

Fig. 2. Intersection of the two planes containing the aryl ring and carboxy-formate group in the title compound

Intermolecular O-H···O and O-H···N interactions are among the intriguing characteristics that stabilize the crystal structure. A strong intermolecular O-H···O interaction of the type O5-H2···O3 of results in arrangement of carboxyformate groups in head to tail fashion along *b*-axis as shown in Fig. 3. On the other hand, O7-H1···O4 hydrogen bond results in forming bridge between the two antiparallel chains of carboxy-formate molecules this can be viewed along *c*-axis (Fig. 4). In addition, a strong N1-H1C···O7 dimes can also be seen in unit cell packing diagram. The molecular packing is further stabilized by carbonyl π-π stacking interactions between 4-(ethoxy-carbonyl)benzenaminium rings along *c*-axis with the inter-planar distances between the two rings being 3.343(3) Å. In addition, π-ring interactions of the type C-H···Cg (Cg being the centroid of the rings) are also observed in the crystal structure (Fig. 3). The extensive packing in the crystal lattice facilitated by O-H···O and N-H···O interactions is shown in Fig. 5. The O-H···O, N-H···O and π-π stacking interactions form molecular two-dimensional sheets along *b*-axis.

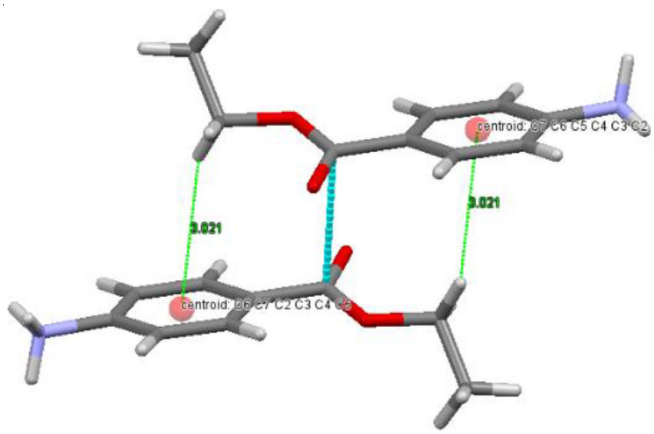

Fig. 3. π-π stacking interaction along *b*-axis in the title compound

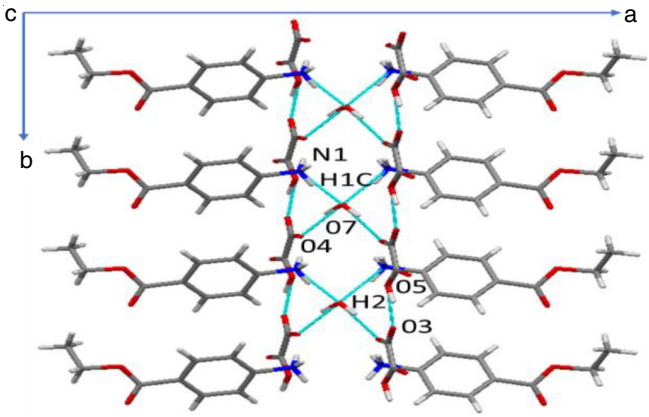

Fig. 4. A unit cell packing of the title compound showing intermolecular O–H···O and O–H···N interactions with dotted lines

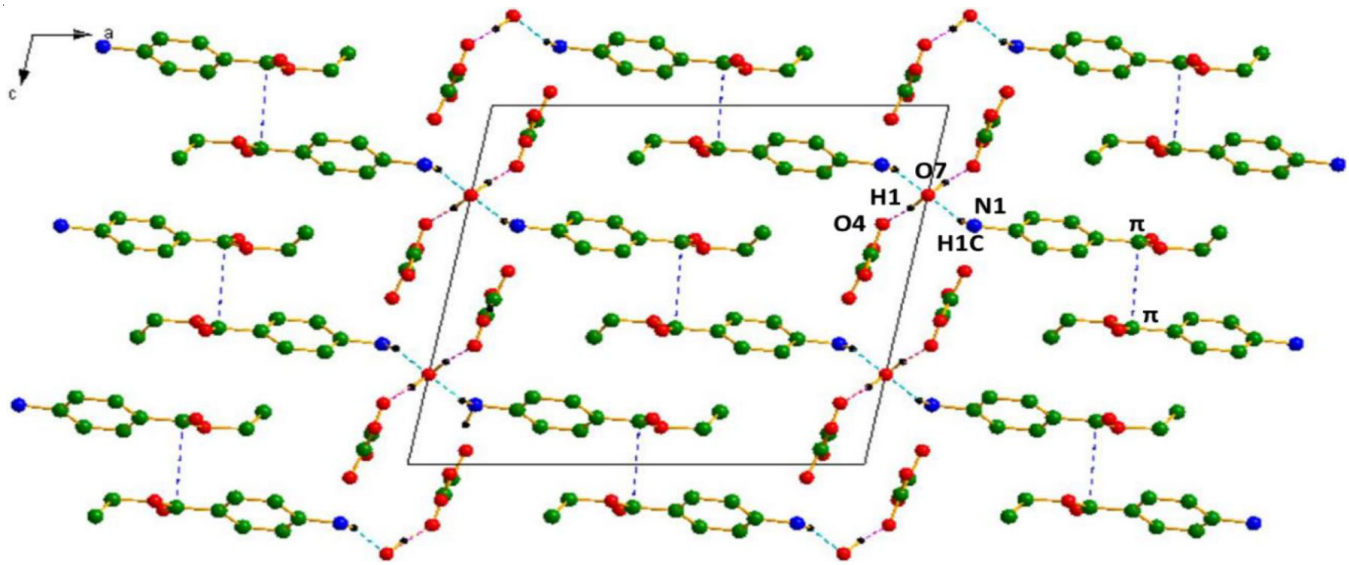

Fig. 5. A view of molecular packing in the title compound along *a*-*c* diagonal

Hirshfeld surfaces: Hirshfeld surfaces are used to visualize the different intermolecular interactions in the molecular packing and its related 2D fingerprint plots helps in a quantitative understanding. The Hirshfeld surface depicts the intermolecular interactions of molecular structure in three dimensions within a crystalline environment. The Hirshfeld surface is shown in Fig. 6 together with maps of d_i and d_e. Oxalic acid and ethyl-4-amino benzoate intermolecular interactions are readily visible on the d_{norm} surface as a bright red spot. For title compound, 2D finger print plots were developed by incorporating reciprocal contacts to illustrate the intermolecular interactions that are specific to a particular crystal structure at the same time. Fig. 7 depicts the calculated numerous contacts that contribute to the stability of the structure. The

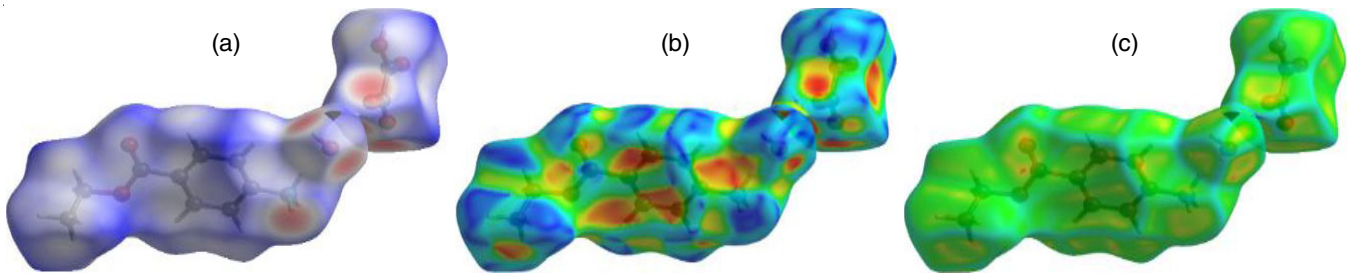

Fig. 6. d_{norm} surface (a), shape index (b) and (c) curved surface plot structure of ethyl-4-amino benzoate oxalate monohydrate

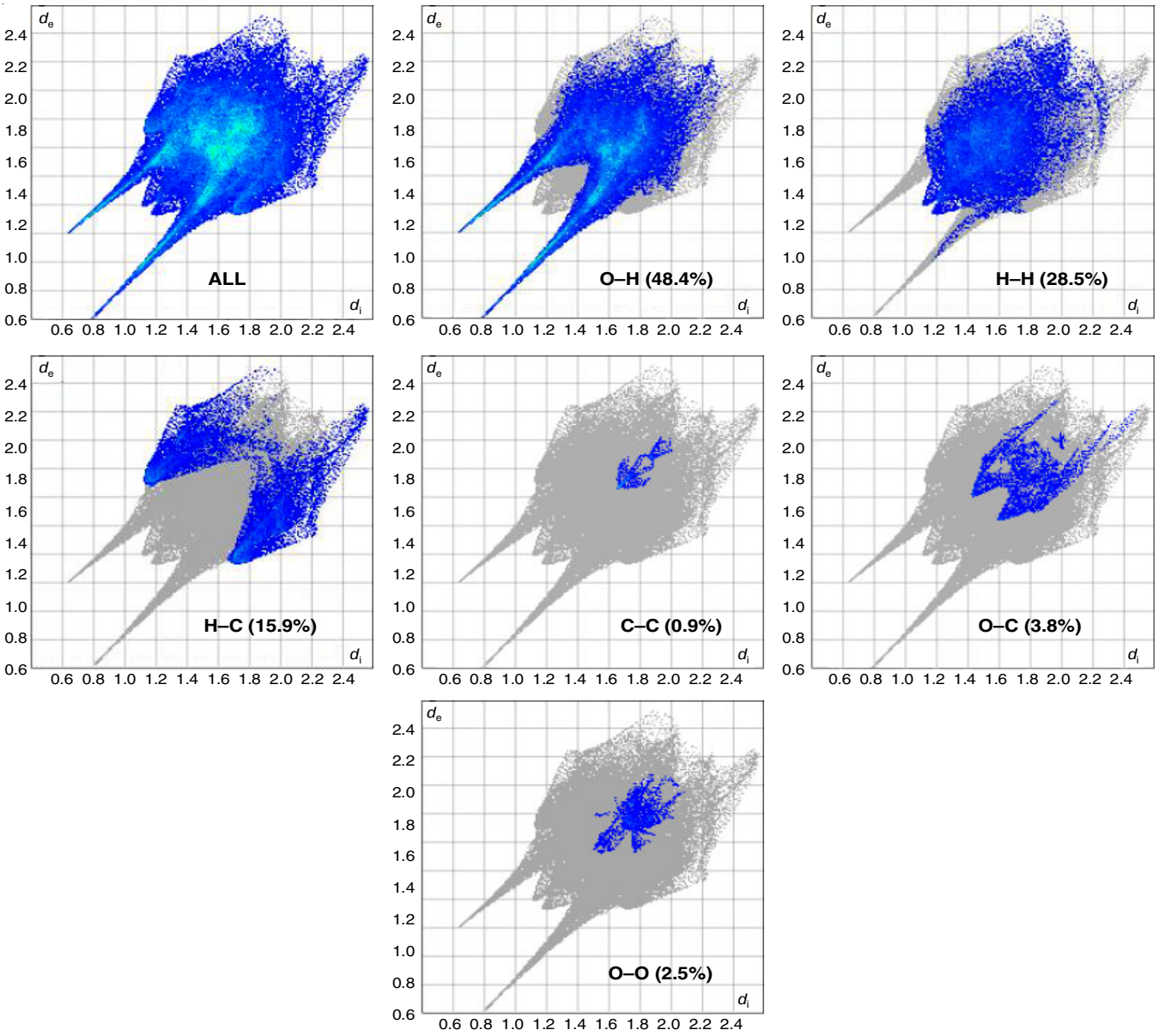

Fig. 7. 2D fingerprint plots of structure of ethyl-4-amino benzoate oxalate monohydrate

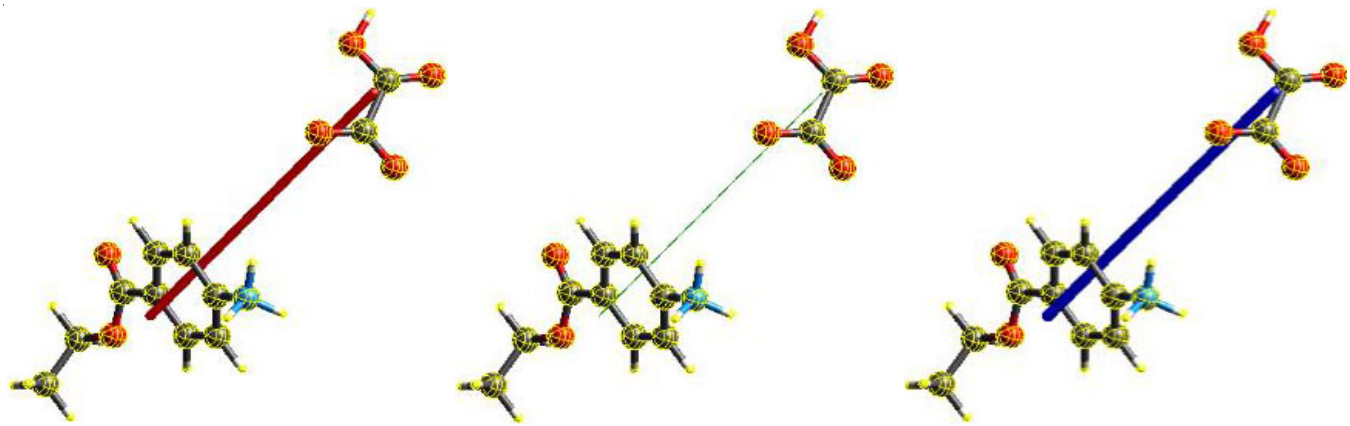

Fig. 8. Electrostatic, dispersion, and total energy frameworks along *a*, *b*, and *c*-axis for the title compound, which correspond to the various energy components. All of the energy frameworks utilised tubes with a scale factor of 300

two spikes in the 2D fingerprint map for the title compound's N-H···O and O-H···O hydrogen bond intermolecular interactions account for 48.4% of the compound's total Hirshfeld surface. The H-H interaction, which accounts for 28.5% of the scattered points with a centre spike in the middle, also contributes significantly to the surface. The other H-C, C-C, O-C and O-O contacts, in addition to the aforementioned primary interactions, also contribute to the total Hirshfeld surfaces of the ethyl-4-aminobenzoate oxalate monohydrate Salt salt. The stability and strength of the multi-component salt have been established by the use of Crystal Explorer 17 energy framework calculations. To determine the energies of the intermolecular interactions between the molecular pairs, a molecular cluster with a radius of 3.8 Å was created around the core molecule. The system's overall interaction energy was found to be -17.1 kJ mol^{-1}, dispersion energy (E_{dis} = -0.9 kJ mol^{-1}), repulsive energy (E_{rep} = 0.0 kJ mol^{-1}), polarization (E_{pol} = -0.6 kJ mol^{-1}) and electrostatic energy (E_{ele} = -7.0 kJ mol^{-1}) [19,20].

3D Energy frameworks: Calculations and generation of interaction energy and interactions in crystal packing are done using the energy frameworks method (Fig. 8).

DFT analysis: Density functional theory (DFT) calculations are essential for theoretical investigations of organic molecules and related domains [21-24]. Furthermore, the DFT technique is an extremely important and useful tool for studying the relationship between chemical compound geometry and electrical properties [25,26]. As a result, in this study, we give DFT calculations for UV spectrum analysis, electronic spectra, HOMO-LUMO energy with different chemical reactivity parameters, molecule electrostatic potential and more.

Computational specifics: The molecular structure was sketched using Gauss View software [27] (Fig. 9). The complete molecular geometry of the compound was optimized using B3LYP density functional theory [28] and a 6-311G++(d, p) basis set with the Gaussian 09W software package [29,30]. Using the crystal optimized structure, the Gaussian 09W programm was used to determine the molecular electrostatic potential, the highest occupied and lowest unoccupied molecular orbital energy (Fig. 9).

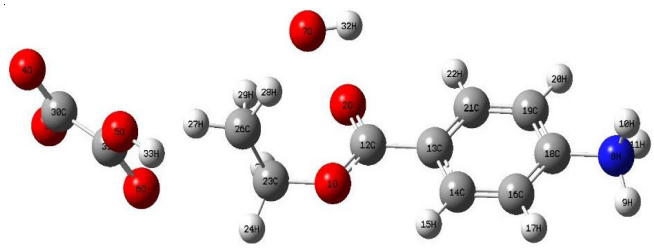

Fig. 9. Optimized molecular structure of ethyl-4-amino benzoate oxalate monohydrate

UV-visible and DOS spectral analysis: In this study, the electronic transition for the crystal was calculated using the B3LYP technique, with the base 6-311++G (d, p) set to UV-visible spectral computation and the gaseous phase added. The theoretical UV-visible absorption spectrum was measuredin the gaseous phase between 300 and 800 nm. The results of the Gauss Sum software [30] analysis of key contributions to electronic transfers are summarized in Table-2. Excitaion energies E (eV) and oscillator strengths (f) were also measured, as well as experimental absorption wavelength (nm) and major

TABLE-2
ABSORPTION WAVELENGTH (λ, nm), EXCITATION ENERGIES (E, ev) AND OSCILLATOR STRENGTHS (f)
THEORETICAL ELECTRONIC ABSORPTION SPECTRA USING THE PROCESS TD-DFT/B3LYP/6-311++ (d, p)

Molecule	λ (nm) computed	E (eV)	*f* (a.u)	Major contribution
Ethyl-4-amino benzoate oxalate monohydrate (E4ABOM)	383	3.51	0.790	HOMO (B) -> LUMO (B) (99%)
	362	3.52	0.030	H-3(B) -> L+1(B) (10%), HOMO (B) -> L+1(B) (11%), HOMO (B) -> L+2(B) (88%)
	359	4.22	0.380	H-3(B) -> L+1(B) (75%), HOMO (B) -> L+1(B) (39%), HOMO (B) -> L+2(B) (13%)
	337	4.35	0.026	H-3(B) -> L+1(B) (14%), HOMO (B) -> L+1(B) (76%)
	323	4.39	0.041	H-2(B) -> L+1(B) (95%)
	307	4.90	0.072	HOMO (B) -> L+3(B) (100%)

contribution (HOMO-LUMO). Fig. 10a-b depict a pictorial representation of theoretical UV-visible spectra and a DOS chart. While the investigated ethyl-4-aminobenzoate oxalate monohydrate exhibited six absorption bands at 383, 362, 359, 337, 323 and 307 nm, which may be attributed to the aromatic, amino benzoate anion, monohydrate and oxalate moiety, respectively, which could be contributed to the $\pi\rightarrow\pi^*$, $n\rightarrow\pi^*$, $\sigma\rightarrow\sigma^*$ transition. The DFT computed wavelength agrees well with the observed wavelength as a result of the findings.

Frontier molecular orbital (FMO) analysis: The HOMO and LUMO energy values can be used to determine a molecule's ability to donate and receive electrons. Frontier molecular orbitals (FMOs) energies such as $A = -E_{LUMO}$ and $I = -E_{HOMO}$ according to Koopmans' definition, measure the ionization potential (I) and electron affinity (A). Global hardness $\eta = 1/2(E_{LUMO}-E_{HOMO})$ [31], chemical potential $\mu = 1/2(E_{LUMO} + E_{HOMO})$, global electrophilicity $\omega = \mu^2/2$ and global softness $S = 1/\eta$. Ionization potential, electron affinity, global softness, global hardness, chemical potential and global electrophilic index of the crystal are all assessed and the data is summarized in Table-3. The electrons occupied and unoccupied (electron affinity and donating) sites are shown in 3D representations of FMO orbitals in different α and β transitions (HOMO-LUMO) levels in Fig. 11a-b.

Potential and density distribution analysis: The MESP surface is very well suited for identifying one molecule by another *via* this potential, as illustrated in Fig. 12. The levels of electrostatic potential at the surface are represented by various colour in the following order: red < orange < yellow < green < blue. In the titled compound, the colour code for these maps ranges from -1.350e-2 (deepest red) to +1.350e-2 (deepest blue), with blue representing the most electropositive, *i.e.* electron poor region and red representing the most electronegative, *i.e.* electron rich region. Clearly, the three oxygen atoms, which serve as an electron donor, are the most electronegative part of the molecule.

TABLE-3
FMO ELECTRONIC PROPERTIES OF ETHYL-4-AMINO BENZOATE OXALATE MONOHYDRATE

	B3LYP_6–311++G(d,p)	
Electronic spatial extent (au)	9972.25	
Nuclear repulsion energy (Hartree)	1366.12	
Rotational coefficients (GHz)	1.2530	
	0.1018	
	0.1013	
Spin	Doublet	
	α-MOs	β-MOs
ELUMO (eV)	-5.648	-4.090
EHOMO (eV)	-3.808	-3.815
ELUMO/HOMO (eV)	1.483	1.072
Ionization-potential (I) (eV)	3.08	3.815
Electron-Affinity (A) (eV)	5.648	4.090
Hardness (η) (eV)	0.916	0.1377
Chemical potential (?) (eV)	-4.728	-3.952
Electrophilic index (ψ)(eV)	12.20	56.71
Softness (ζ) (eV^{-1})	1.0917	7.262

Conclusion

This study involves the synthesis, crystallization and 3D structure confirmation of ethyl-4-amino benzoate oxalate monohydrate salt using the single crystal X-ray diffraction method. Additionally, the computational Hirshfeld surfaces method was used to analyze the crystal packing (intermolecular interactions). Intermolecular interaction of the type O-H···O and O-H···N stabilize the crystal structure. Through interactions between 4-(ethoxycarbonyl)benzenaminium rings, the molecular packing is further stabilized. Additionally, C-H···Cg interactions between π-rings, with Cg serving as the centroid of the rings, are observed in the crystal structure. For the title molecule, the intercontact O···H (48.4%) contributes more to the Hirshfeld surfaces. According to the crystal structure, the formation of the salt is caused by a proton transfer from the

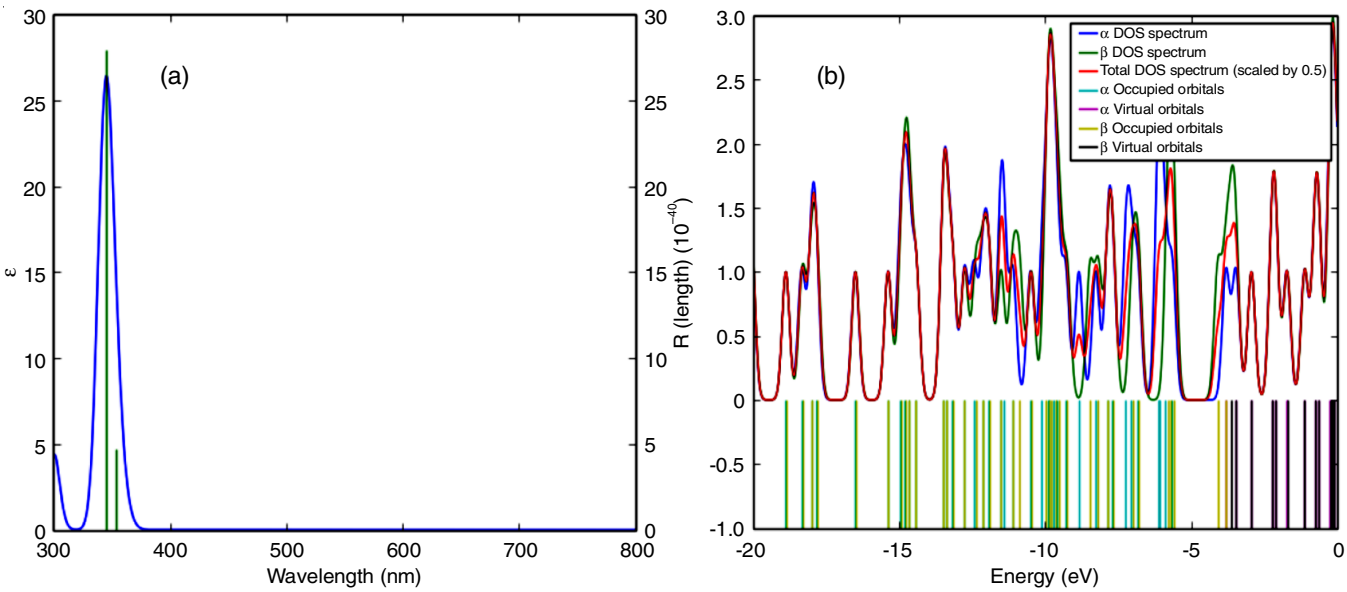

Fig. 10. Theoretical UV-vis spectra (a) & DOS (b) spectra of the ethyl-4-amino benzoate oxalate monohydrate

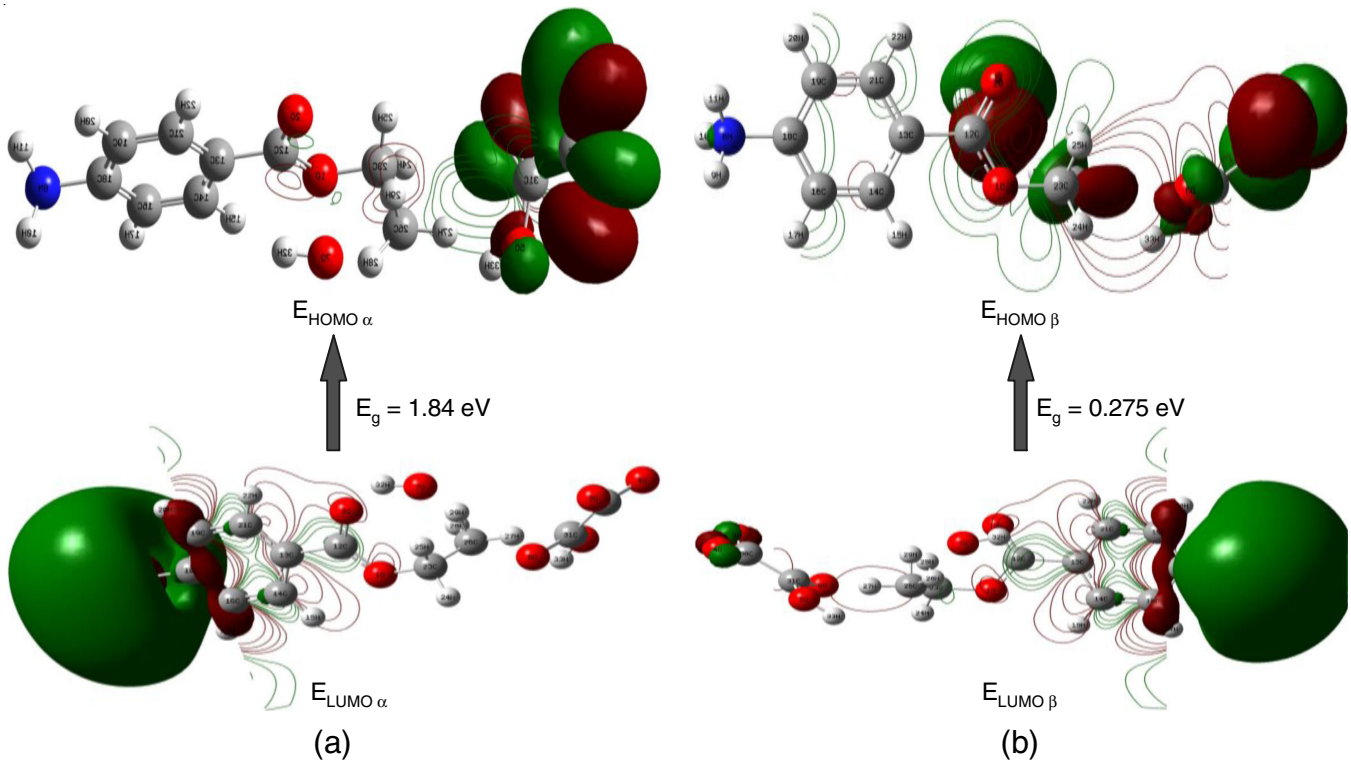

Fig. 11. DFT/B3LYP/6–31G (d,p) -3D representation of FMO orbitals in different α (a) and β (b) transitions (HOMO-LUMO) level

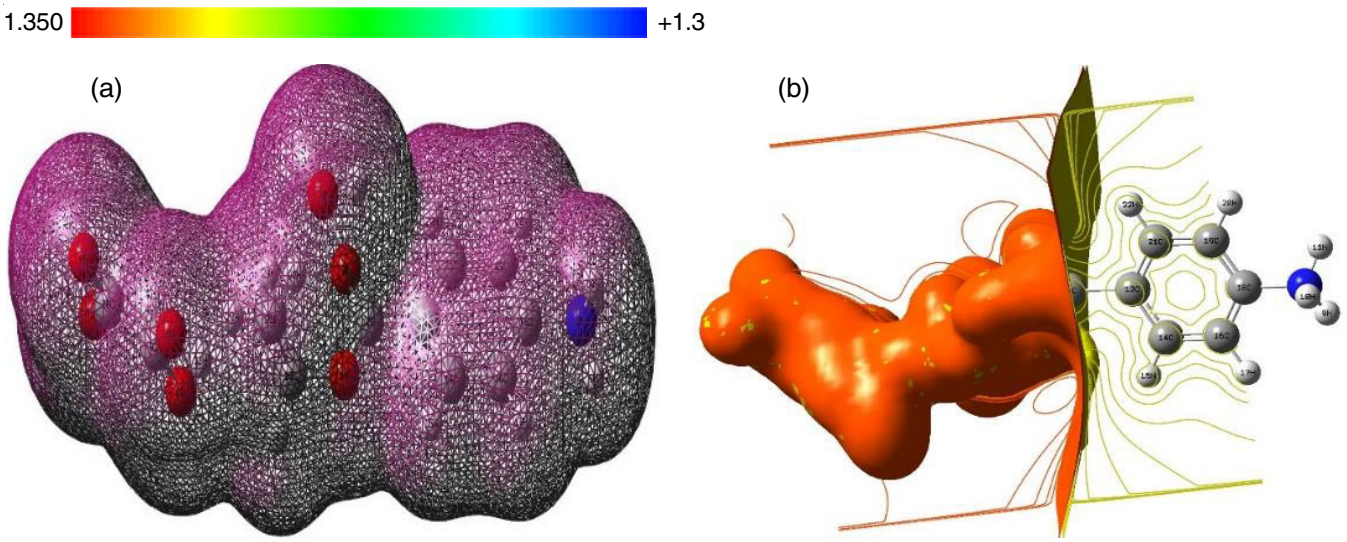

Fig. 12. (a) & (b) Potential distribution mapping and electron density total SCF of studied crystal

phenolic group of oxalic acid to the amine group of ethyl-4-aminobenzoate. The extensive UV-vis spectrum and DFT data validated the structure of the chemically synthesized studied crystal. The crystal is clear in the visible portion of its spectrum, according to TD-DFT analysis. The optical energy gap (DOS spectra and HOMO-LUMO), chemical reactivity (GCRD) and charge distribution (electron density and MEP plots) all indicate that the crystal is NLO active. The UV-vis optical analysis supports the stability and hyper-conjugative interactions of the molecule. The experimental and computational analysis provides extensive evidence that this material exhibits all the necessary features for use in NLO devices.

Supplementary material: Crystallographic data for the compound has been deposited with the Cambridge Crystallographic Data Centre as supplementary publication number CCDC 2089478 Copies of this information may beobtained free of charge *via* www. ccdc.cam.ac.uk /conts/ retrieving.html (or from the CCDC, 12 Union Road, Cambridge CB2 1EZ, UK; fax: +44-1223-336033; e-mail: deposit@ccdc.cam.ac.uk).

ACKNOWLEDGEMENTS

The authors thanks to DST PURSE Phase II, Department of Chemistry, Annamalai University for Single Crystal XRD Analysis.

CONFLICT OF INTEREST

The authors declare that there is no conflict of interests regarding the publication of this article.

REFERENCES

1. A. Iwan, P. Bilski, H. Janeczek, B. Jarzabek, M. Domanski, P. Rannou, A. Sikora, D. Pociecha and B. Kaczmarczyk, *J. Mol. Struct.*, **963**, 175 (2020); https://doi.org/10.1016/j.molstruc.2009.10.031
2. A. Longarte, J.A. Fernandez, I. Unamuno and F. Castano, *Chem. Phys.*, **260**, 83 (2000); https://doi.org/10.1016/S0301-0104(00)00164-6
3. S.M. Kumar, B.C. Manjunath, G.S. Lingaraju, M.M.M. Abdoh, M.P. Sadashiva and N.K. Lokanath, *Crystal. Struct. Theo. Appl.*, **2**, 124 (2013); https://doi.org/10.4236/csta.2013.23017
4. N.K. Manjunatha, S.M. Kumar, M.T. Swamy, B.P. Siddaraju and N.K. Lokanath, *Chemical Data Coll.*, **27**, 100377 (2020); https://doi.org/10.1016/j.cdc.2020.100377
5. S.M. Kumar, A.-O. Fares Hezam, B.C. Manjunath, V.R. Shamprasad, Y.H. Eissa Mohammed, N. Mahesh, Zabiulla, A.K. Shaukath, N.K. Lokanath and K. Byrappa, *J. Mol. Struct.*, **1156**, 216 (2018); https://doi.org/10.1016/j.molstruc.2017.11.094
6. M. Udayakumar, K. Jagatheeswaran, S.S. Ganesan, N.S. Venkataramanan, S. Madan Kumar, K. Byrappa and S. Thamotharan, *J. Mol. Struct.*, **1133**, 510 (2017); https://doi.org/10.1016/j.molstruc.2016.11.082
7. P. Guerrieri, A.C.F. Rumondor, T. Li and L.S. Taylor, *AAPS PharmSciTech*, **11**, 1212 (2010); https://doi.org/10.1208/s12249-010-9499-4
8. Rigaku, Rigaku Corporation, Tokyo, Japan (2011).
9. G.M. Sheldrick, *Acta Crystallogr. A*, **64**, 112 (2008); https://doi.org/10.1107/S0108767307043930
10. A.L. Spek, *Acta Cryst.*, **A46**, c34 (1990); https://doi.org/10.1107/S0108767390099780
11. C.F. Macrae, I.J. Bruno, J.A. Chisholm, P.R. Edging-ton, P. McCabe, E. Pidcock, L. Rodriguez-Monge, R. Taylor, J. van de Streek and P.A. Wood, *J. Appl. Cryst.*, **41**, 466 (2008); https://doi.org/10.1107/S0021889807067908
12. L.J. Farrugia, *J. Appl. Cryst.*, **45**, 849 (2012); https://doi.org/10.1107/S0021889812029111
13. S. Suda, A. Tateno, D. Nakaneorcid and T. Akitsuorcid, *Int. J. Org. Chem.*, **13**, 57 (2023); https://doi.org/10.4236/ijoc.2023.132006
14. Y.H. Ma, S.W. Ge, W. Wang and B.W. Sun, *J. Mol. Struct.*, **1097**, 87 (2015); https://doi.org/10.1016/j.molstruc.2015.05.014
15. M.A. Spackman and D. Jayatilaka, *CrystEngComm*, **11**, 19 (2009); https://doi.org/10.1039/B818330A
16. M.J. Turner, J.J. McKinnon, S.K. Wolff, D.J. Grimwood, P.R. Spackman, D. Jayatilaka and M.A. Spackman, CrystalExplorer17, University of Western Australia (2017).
17. S.M. Kumar, A.K. Kudva, B.C. Manjunath, P. Naveen, T. Prashanth, S.A. Khanum, N.K. Lokanath and P. Nagendra, *Chem. Data Collect.*, **19**, 100168 (2019); https://doi.org/10.1016/j.cdc.2018.11.010
18. S.M. Kumar, *Heliyon*, **5**, e01209 (2019); https://doi.org/10.1016/j.heliyon.2019.e01209
19. S. Madan Kumar, B.N. Lakshminarayana, S. Nagaraju, S. Sushma, S. Ananda, B.C. Manjunath, N.K. Lokanath and K. Byrappa, *J. Mol. Struct.*, **1173**, 300 (2018); https://doi.org/10.1016/j.molstruc.2018.06.083
20. S. Madan Kumar, B.C. Hemraju, S.M. Anil, N.K. Manjunatha, M.T. Swamy, N.K. Lokanath, M. Al-Ghorbani, N. Al-Zaqri and A. Alsalme, *Z. Kristallogr. Cryst. Mater.*, **235**, 85 (2020); https://doi.org/10.1515/zkri-2019-0065
21. P. Hohenberg and W. Kohn, *Phys. Rev.*, **136(3B)**, B864 (1964); https://doi.org/10.1103/PhysRev.136.B864
22. W. Kohn and L.J. Sham, *Phys. Rev.*, **140(4A)**, A1133 (1965); https://doi.org/10.1103/PhysRev.140.A1133
23. S.M. Hiremath, A. Suvitha, N.R. Patil, C.S. Hiremath, S.S. Khemalapure, S.K. Pattanayak, V.S. Negalurmath and K. Obelannavar, *J. Mol. Struct.*, **1171**, 362 (2018); https://doi.org/10.1016/j.molstruc.2018.05.109
24. A. Suvitha, S. Periandy, S. Boomadevi and M. Govindarajan, *Spectrochim. Acta A Mol. Biomol. Spectrosc.*, **117**, 216 (2014); https://doi.org/10.1016/j.saa.2013.07.080
25. M. Evecen and H. Tanak, *Mater. Sci. Pol.*, **34**, 886 (2016); https://doi.org/10.1515/msp-2016-0115
26. S. Naseem, M. Khalid, M.N. Tahir, M.A. Halim, A.A.C. Braga, M.M. Naseer and Z. Shafiq, *J. Mol. Struct.*, **1143**, 235 (2017); https://doi.org/10.1016/j.molstruc.2017.04.093
27. R.D. Dennington, T.A. Keith and J.M. Millam, Semichem Inc. (2016).
28. C. Lee, W. Yang and R.G. Parr, *Phys. Rev. B Condens. Matter*, **37**, 785 (1988); https://doi.org/10.1103/PhysRevB.37.785
29. M.J. Frisch, G.W. Trucks, H.B. Schlegel, G.E. Scuseria, M.A. Robb, J.R. Cheeseman, G. Scalmani, V. Barone, B. Mennucci, G.A. Petersson, H. Nakatsuji, M. Caricato, X. Li, H.P. Hratchian, A.F. Izmaylov, J. Bloino, G. Zheng, J.L. Sonnenberg, M. Hada, M. Ehara, K. Toyota, R. Fukuda, J. Hasegawa, M. Ishida, T. Nakajima, Y. Honda, O. Kitao, H. Nakai, T. Vreven, J.A. Montgomery, Jr., J.E. Peralta, F. Ogliaro, M. Bearpark, J.J. Heyd, E. Brothers, K.N. Kudin, V.N. Staroverov, R. Kobayashi, J. Normand, K. Raghavachari, A. Rendell, J.C. Burant, S.S. Iyengar, J. Tomasi, M. Cossi, N. Rega, J.M. Millam, M. Klene, J.E. Knox, J.B. Cross, V. Bakken, C. Adamo, J. Jaramillo, R. Gomperts, R.E. Stratmann, O. Yazyev, A.J. Austin, R. Cammi, C. Pomelli, J.W. Ochterski, R.L. Martin, K. Morokuma, V.G. Zakrzewski, G.A. Voth, P. Salvador, J.J. Dannenberg, S. Dapprich, A.D. Daniels, Ö. Farkas, J.B. Foresman, J.V. Ortiz, J. Cioslowski and D.J. Fox, Gaussian, Inc., Wallingford CT (2009).
30. N.M. O'boyle, A.L. Tenderholt and K.M. Langner, *J. Comput. Chem.*, **29**, 839 (2008); https://doi.org/10.1002/jcc.20823
31. M. Pourtabrizi, N. Shahtahmassebi and M.R. Sharifmoghadam, *Opt. Quantum Electron.*, **53**, 1 (2021); https://doi.org/10.1007/s11082-020-02634-9